Journal of Magnetic Resonance 200 (2009) 334–339

Contents lists available at ScienceDirect

Journal of Magnetic Resonance

journal homepage: www.elsevier.com/locate/jmr

Optimum excitation of "enhanced" central transition populations

Nicole M. Trease, Krishna K. Dey, Philip J. Grandinetti *

Department of Chemistry, The Ohio State University, 120 W. 18th Avenue, Columbus, OH 43210-1173, USA

ARTICLE INFO

Article history:
Received 1 June 2009
Revised 15 July 2009
Available online 18 July 2009

Keywords:
Solid-state NMR
Quadrupole nuclei
Sensitivity enhancement

ABSTRACT

Central transition (CT) sensitivity enhancement schemes that transfer polarization from satellites to the CT through selective saturation or inversion of neighboring satellite transitions have provided a welcome improvement for magic-angle spinning spectra of half-integer quadrupole nuclei. While many researchers have investigated and developed different methods of creating enhanced CT populations, here we investigate the conversion of these enhanced CT populations into observable CT coherence. We show a somewhat unexpected result that a conversion pulse length optimized for maximum sensitivity on equilibrium populations may not be optimum for an enhanced (non-equilibrium) polarization. Furthermore, CT enhancements can be lost if excessive rf field strength is used to convert this enhanced polarization into CT coherence. While a maximally enhanced CT signal is expected when using a perfectly selective CT conversion pulse, we have found that significant sensitivity loss can occur when using surprisingly low rf field strengths, even for sites with relatively large quadrupole coupling constants. We have systematically investigated these issues, and present some general guidelines and expectations when optimizing the conversion of enhanced (non-equilibrium) CT populations into observable CT coherence.

1. Introduction

Recent use of preparatory pulse sequences to transfer polarization from the satellite transitions to the central transition (CT) has greatly improved the sensitivity of magic-angle spinning (MAS) spectra for the CT of half-integer quadrupole nuclei in polycrystalline samples. These sequences can generally be divided into two classes, depending on whether the target state is selective satellite saturation (e.g., rotor-assisted population transfer (RAPT) [1–3] and double frequency sweeps (DFS) [4]), or selective satellite inversion [5] (e.g., hyperbolic secant (HBSec) [6] and WURST [7]). While optimization approaches vary amongst sequences, and also between samples, the general goal has been to maximize the excitation of the satellite transitions while minimizing any excitation of the central transition. While selective satellite inversion can potentially provide a higher sensitivity enhancement than selective satellite saturation, its implementation is more challenging as it requires selective adiabatic inversion of a single spinning sideband of the satellite transition [7].

In contrast to optimization of the population transfer, little attention has been paid to the optimum conversion of the enhanced CT population into observable CT coherences. Here we show a somewhat unexpected result that a conversion pulse length optimized on equilibrium populations will *not* be optimal for converting enhanced CT populations into observable CT coherences. Additionally, a significant sensitivity enhancement can be lost if excessive rf field strength is used when converting an enhanced central transition population into coherence. We have explored the nutation behavior of enhanced central transition populations from low ($\omega_1 \ll \omega_q$) to high ($\omega_1 \gg \omega_q$) radio frequency (rf) field strength, and show that the onset of sensitivity loss occurs at surprisingly lower rf field strength than expected, even for sites with relatively large quadrupole coupling constants. A theoretical explanation of these effects is presented and illustrated through numerical simulations.

2. Methods

All NMR measurements were done at 9.4 T, using a homebuilt 4 mm DAS probe [8]. Radio frequency field strengths were calibrated using ^{87}Rb in RbCl and ^{23}Na in NaCl. The frequency switched Gaussian (FSG)-RAPT [2] sequence in Fig. 1A was used to enhance the central transition populations through selective saturation of the satellite transition. The optimized FSG-RAPT pulse parameters were $\omega_{off}/2\pi = 570$ kHz, $n = 500$ and a Gaussian pulse length of 15 μs ($\sigma = 1.53$ μs) in the $^{87}RbClO_4$ experiments, and $\omega_{off}/2\pi = 120$ kHz, $n = 15$, $\omega_{rf}/2\pi = 33$ kHz and a Gaussian pulse length of 100 μs ($\sigma = 16.5$ μs) in the $^{23}NaNO_3$ experiments. Selective inversion of satellite transitions was performed with adiabatic passage through a single satellite transition spinning sideband using a WURST pulse [7] as shown in Fig. 1B. In the $^{23}NaNO_3$ experiments, the WURST

E-mail address: grandinetti.1@osu.edu (P.J. Grandinetti).
URL: http://www.grandinetti.org (P.J. Grandinetti).

1090-7807/$ - see front matter © 2009 Elsevier Inc. All rights reserved.
doi:10.1016/j.jmr.2009.07.020

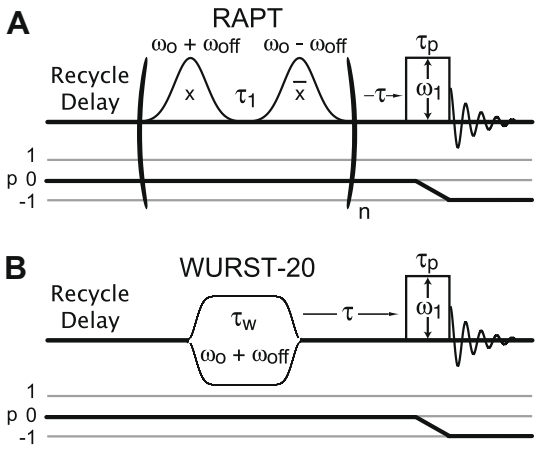

Fig. 1. (A) Frequency switched Gaussian-RAPT sequence for selective satellite saturation with ω_{off} optimal at $\omega_q/4$ for a spin-3/2 nuclei. (B) Selective satellite inversion using a WURST-20 (adiabatic) pulse swept through a single spinning sideband of the satellite transition.

pulse was applied to the 8th spinning side band ($\omega_{off}/2\pi$ = 80 kHz) with an excitation width of 10 kHz, τ_w = 5 ms and $\omega_{rf}/2\pi$ = 5.7 kHz.

We define the experimental enhancement factor as the ratio of the CT signal area obtained with enhanced populations to the CT signal area obtained with equilibrium populations,

$$\eta = \frac{\int S^{CT}_{enhanced}(\omega)\,d\omega}{\int S^{CT}_{eq}(\omega)\,d\omega}. \tag{1}$$

As we will show, however, this definition is somewhat problematic, since a CT signal obtained with enhanced populations and measured using a conversion *pulse length optimized on equilibrium populations*, is not as strong as when using a conversion *pulse length optimized on the enhanced populations*.

To assist in our analysis, full density operator numerical simulations [9] were performed, using three different initial density operators, $\hat{\rho}_{eq}$, $\hat{\rho}_{sat}$, and $\hat{\rho}_{inv}$, corresponding to equilibrium, selective satellite saturation, and selective satellite inversion, respectively. For each initial density operator a series of two-dimensional nutation experiments [10] were calculated at different rf field strengths. The results of these simulations are shown and discussed in the next section.

3. Discussion

Fig. 2 highlights the problem with using excessive field strength for the rf pulse that converts enhanced central transition populations into coherence. This figure contains ^{87}Rb central transition spectra in $RbClO_4$ obtained from equilibrium and FSG-RAPT enhanced populations as a function of the rf field strength used to convert the central transition population into observable signal. Under ideal conditions, the FSG-RAPT enhanced population should yield a signal enhancement of 2.0. In Fig. 2 the enhancement decreases from 1.96 to 1.49 as the CT conversion pulse field strength increases from 7.8 kHz to 65 kHz.

To better understand the mechanism behind this signal loss, we examine the evolution of the initial density operator during an rf pulse. To a good approximation, the Hamiltonian governing this process is given by

$$\hat{H}/\hbar = \omega_q A_{20}\hat{T}_{20} - \omega_1\hat{I}_x, \tag{2}$$

where ω_1 is the rf field strength, and the quadrupole splitting, ω_q, is given by

$$\omega_q = 6\pi C_q/2I(2I-1), \tag{3}$$

with C_q as the quadrupole coupling constant and A_{20} as an irreducible spherical tensor element describing the orientation of the quadrupole coupling principal axis system.

In the limit of low rf field strength, $\omega_1 \ll \omega_q$, this Hamiltonian, written in terms of fictitious spin half operators [11,12] for the I = 3/2 case, can be approximated to first order [11,13] in ω_1 as:

$$\hat{H}/\hbar \approx \sqrt{\frac{3}{2}}\omega_q A_{20}\left(\hat{E}^{1-4} - \hat{E}^{2-3}\right) - 2\omega_1\hat{I}_x^{2-3}. \tag{4}$$

In this low rf field strength limit, we find the well-known result that the central transition for spin I = 3/2 nutates at a frequency of $2\omega_1$, and, more generally, one can show that it will nutate at $(I+\frac{1}{2})\omega_1$ for arbitrary spin I.

With the bandwidth of the NMR receiver narrowed so only the central transition is detected, the nutation signal strength in the low field strength limit (see Appendix A) is given by

$$S(\tau_p) = 2\,\mathrm{Tr}\left[\hat{\rho}(0)\hat{I}_z^{2-3}\right]\sin(2\omega_1\tau_p), \tag{5}$$

where τ_p is the duration of the pulse. Thus, the three initial states

$$\hat{\rho}_{eq}/b = 3\hat{I}_z^{1-4} + \hat{I}_z^{2-3}, \tag{6a}$$

$$\hat{\rho}_{sat}/b = 2\hat{I}_z^{1-4} + 2\hat{I}_z^{2-3}, \tag{6b}$$

$$\hat{\rho}_{inv}/b = \hat{I}_z^{1-4} + 3\hat{I}_z^{2-3}, \tag{6c}$$

where $b = \hbar\omega_0/k_B T(2I+1)$, will have identical nutation frequencies, reaching their first maximum at $\omega_1\tau_p = \pi/4$ with relative signal strengths of 1, 2, and 3, respectively.

In Fig. 3 is a comparison of the experimental nutation curves at low rf field strength, $\omega_1/2\pi$ = 0.660 kHz for the ^{23}Na site ($\omega_q/2\pi$ = 170 kHz) in $NaNO_3$, for these three initial states along with those calculated from Eqs. (5) and (6). As predicted, the experimen-

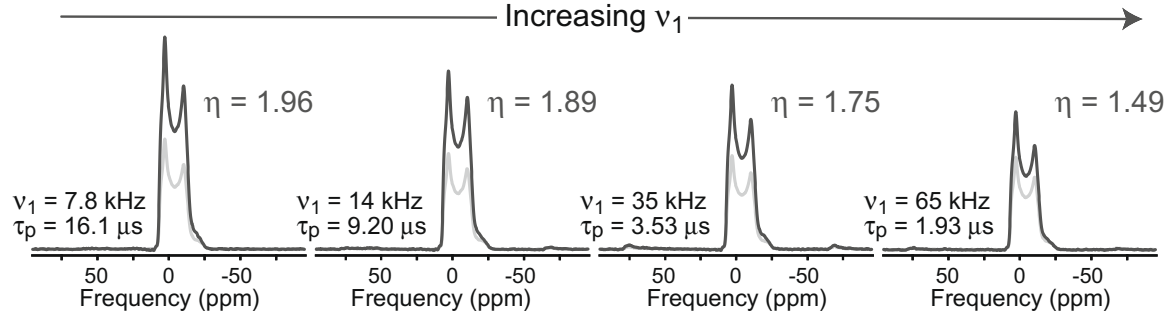

Fig. 2. The enhanced CT signal is lost with increasing ω_1 of the CT conversion pulse. From left to right is a comparison of the FSG-RAPT-echo and echo pulse sequences for increasing ω_1 of the CT of ^{87}Rb in $RbClO_4$ with C_q = 3.2 MHz and η_q = 0.2. A 50% loss of signal is seen as $\omega_1/2\pi$ increases from 7.8 kHz to 65 kHz. Spectra were obtained at $\omega_0/2\pi$ = 130.918 MHz.

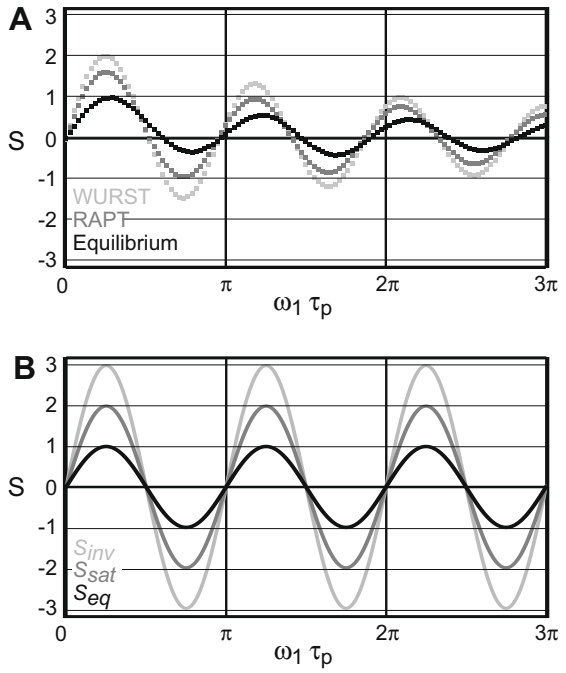

Fig. 3. (A) Experimental central transition nutation curves for ^{23}Na ($I = 3/2$) in $NaNO_3$ ($\omega_q/2\pi = 170$ kHz) using a low rf field strength ($\omega_1/2\pi = 0.7$ kHz) CT conversion pulse. The darkness of the squares decreases for the three experiments from equilibrium (black), RAPT-enhanced (grey) to WURST-enhanced (light grey). (B) Central transition nutation curves calculated for spin-3/2 nuclei when $\omega_1 \ll \omega_q$ using Eq. (5). From the largest to smallest amplitude are the nutation curves for the different density operators, inverted (light grey), saturated (grey) and equilibrium (black), respectively. Note that all three initial states nutate at the same frequency, $(I+\frac{1}{2})\omega_1 = 2\omega_1$ for the central transition.

tal nutation curves of the three initial states have nearly identical frequencies and amplitude maxima that vary from 1 to 1.8 to 2 for the equilibrium, FSG-RAPT, and WURST enhanced populations, respectively. As noted in earlier work [1], the enhancements obtained for strongly dipolar coupled nuclei, such as ^{23}Na, tend to be smaller than those obtained for dilute quadrupole nuclei, such as ^{17}O, where these enhancements are, generally, more valuable.

In contrast to the low rf field strength limit, when $\omega_1 \gg \omega_q$ we are in the high rf field strength limit and the pulse is no longer selective to the central transition. In this limit the Hamiltonian in Eq. (2), to lowest order, can be approximated as,

$$\hat{H}/\hbar \approx -\omega_1 \hat{I}_x. \tag{7}$$

We still treat the bandwidth of the NMR receiver as narrow, detecting only the central transition, so the nutation signal strength in the high field strength limit (see Appendix A) for spin $I = 3/2$ becomes,

$$S(\tau_p) = \frac{2}{\sqrt{5}}\mathrm{Tr}\left[\hat{\rho}(0)\widehat{\mathscr{T}}_{1,0}\right]\sin\omega_1\tau_p - \frac{3}{8\sqrt{5}}\mathrm{Tr}\left[\hat{\rho}(0)\widehat{\mathscr{T}}_{3,0}\right]\{\sin\omega_1\tau_p + 5\sin 3\omega_1\tau_p\}, \tag{8}$$

where the $\widehat{\mathscr{T}}_{l,m}$ are the unit irreducible spherical tensors [9,14]. Here, again, we see a well-known result that first-rank spin order, as found in the equilibrium density operator, will nutate at a frequency of ω_1. Surprisingly, however, we also find a lesser known result that if the enhanced population contains third-rank spin order, the nutation spectrum will also contain a frequency component at $3\omega_1$. One can show that the three initial states in Eq. (6) expressed in terms of unit irreducible spherical tensors (see Appendix A) in the spin $I = 3/2$ case are

$$\hat{\rho}_{eq}/b = \sqrt{5}\widehat{\mathscr{T}}_{10}, \tag{9a}$$

$$\hat{\rho}_{sat}/b = \frac{4}{\sqrt{5}}\widehat{\mathscr{T}}_{10} - \frac{2}{\sqrt{5}}\widehat{\mathscr{T}}_{30}, \tag{9b}$$

$$\hat{\rho}_{inv}/b = \frac{3}{\sqrt{5}}\widehat{\mathscr{T}}_{10} - \frac{4}{\sqrt{5}}\widehat{\mathscr{T}}_{30}. \tag{9c}$$

Thus, combining Eqs. (8) and (9) we obtain the nutation signals for the three initial states,

$$S_{eq}/b = 2\sin\omega_1\tau_p, \tag{10a}$$

$$S_{sat}/b = \frac{7}{4}\sin\omega_1\tau_p + \frac{3}{4}\sin 3\omega_1\tau_p, \tag{10b}$$

$$S_{inv}/b = \frac{3}{2}\sin\omega_1\tau_p + \frac{3}{2}\sin 3\omega_1\tau_p. \tag{10c}$$

More generally, one can show that the nutation spectrum of enhanced non-equilibrium states will contain all odd multiples of ω_1 up to $2I\omega_1$ in the high rf field strength limit (see Appendix A).

In Fig. 4 is a comparison of the experimental nutation curves near the high rf field strength limit ($\omega_1/2\pi = 178$ kHz) for the ^{23}Na site ($\omega_q/2\pi = 170$ kHz) in $NaNO_3$ along with the nutation curves calculated from Eq. (10). The equilibrium state, which nutates at a single frequency of ω_1, reaches its first relative amplitude maximum of 1.75 at $\omega_1\tau_p = \pi/2$. In contrast, the interference between the ω_1 and $3\omega_1$ nutation frequencies causes the maximum signal from the FSG-RAPT and WURST enhanced populations to reach their first maxima of 1.50 and 1.75, respectively, at approximately $\omega_1\tau_p \approx \pi/4$. Notice how the experimental FSG-RAPT and WURST enhanced populations only reach relative amplitudes of 1.02 and 0.5, respectively, at $\omega_1\tau_p = \pi/2$, where a maximum is traditionally expected. The state with inverted satellite transitions loses over 70% of its potential signal strength when detected with

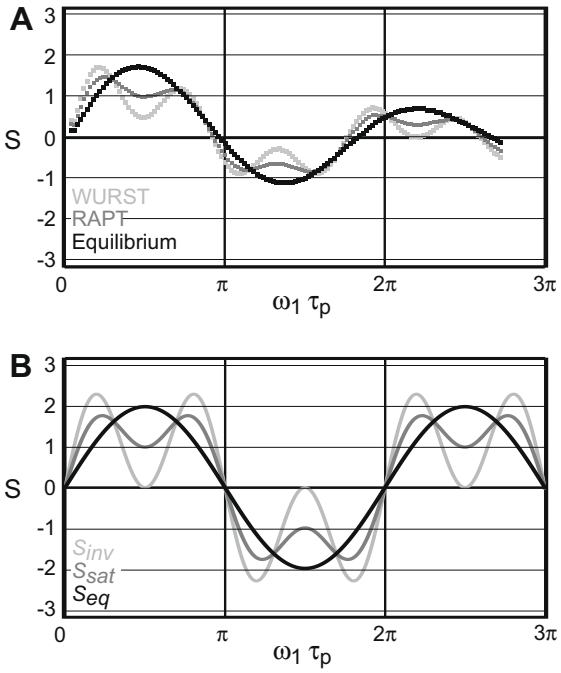

Fig. 4. (A) Experimental central transition nutation curves for ^{23}Na ($I = 3/2$) in $NaNO_3$ ($\omega_q/2\pi = 170$ kHz) using a high rf field strength ($\omega_1/2\pi = 178$ kHz) central transition conversion pulse. The darkness of the squares decreases for the three experiments from equilibrium (black), RAPT-enhanced (grey) to WURST-enhanced (light grey). (B) Central transition nutation curves calculated for spin-3/2 nuclei when $\omega_1 \gg \omega_q$ using Eq. (8). The line darkness decreases for the initial density operators from equilibrium (black), saturated (grey) to inverted (light grey).

a $\pi/2$ pulse. In fact, the simulated nutation signal amplitude in the theoretical high field strength limit for the inverted population goes to zero at $\omega_1\tau_p = \pi/2$. Clearly, in this high rf power regime, significant signal loss will occur unless the conversion pulse length is properly optimized on the enhanced populations. In practice, the experimental approach for optimizing signal strength remains the same regardless of whether equilibrium or enhanced populations are present and whether low or high rf field strength is employed. That is, the experimental signal strengths are plotted as a function of increasing pulse length until clear maximum signal strength is observed. When working with enhanced populations, however, one needs to be aware that the nutation behavior of enhanced populations can markedly differ from that of equilibrium populations.

Conversion pulse length, however, is not the only factor that needs optimization when exciting a central transition with enhanced (non-equilibrium) populations. An additional factor that needs careful consideration is the field strength of the conversion pulse. To illustrate this aspect we show simulated CT signal strengths obtained from equilibrium, saturated, and inverted initial states as a function of conversion pulse field strength and quadrupole splitting in Fig. 5. In Fig. 5A the simulation was performed using a conversion pulse length optimized at each rf field strength on the equilibrium population, and in Fig. 5B the conversion pulse length was optimized at each rf field strength on the enhanced population.

In Fig. 5A the signal strength from an equilibrium initial state, beginning at a normalized value of unity at the lowest rf field strength, reaches a maximum of 2 in the high rf field strength limit, as expected. The signal from the equilibrium initial state rises to 1.5, i.e., half the distance to its maximum value, at $\omega_1 \approx \omega_q/4$. Generally, the central transition signal strength obtained from the equilibrium magnetization will increase by a factor of $I + 1/2$ when increasing the field strength of the conversion pulse from the low ($\omega_1 \ll \omega_q$) to high ($\omega_1 \gg \omega_q$) rf power regime. It is interesting to note that this high field strength "signal enhancement" is identical to the maximum possible RAPT enhancement, although it is less than the maximum possible inverted satellite enhancement. Attempting to use this high field strength limit to obtain a stronger CT signal from equilibrium populations, however, can be quite expensive with regard to amplifiers and probe construction and even then, may not be sufficient for many quadrupole nucleus sites. An attractive feature of the CT population enhancement schemes outlined here is that they work best in the less expensive and easily achievable low rf power regime.

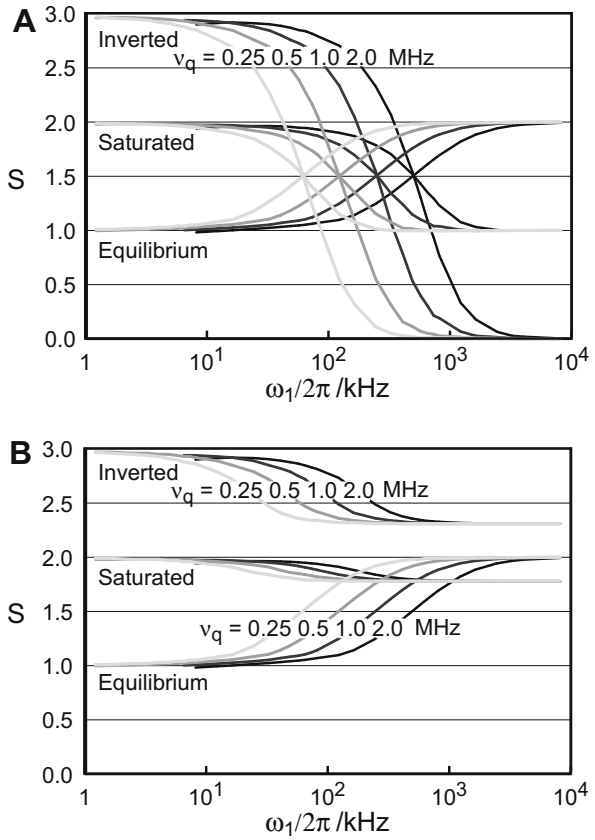

Fig. 5. (A) Simulated CT signal strength of ^{87}Rb for the initial density operators, $\hat{\rho}_{eq}$, $\hat{\rho}_{sat}$ and $\hat{\rho}_{inv}$ as a function of ω_1, CT conversion pulse rf field strength, for $\omega_q/2\pi$ values of 0.25, 0.5, 1.0 and 2.0 (line darkness increases with increasing ω_q). The CT conversion pulse length used was optimized on $\hat{\rho}_{eq}$ at each ω_1. (B) Same as (A) except the CT conversion pulse used was optimized on the enhanced initial density operators to give maximum signal at each ω_1 value.

In Fig. 5A we see that the signal strengths from the saturated and inverted satellite initial states begin at their maximum values of ~2 and ~3, respectively, and decrease to their minimum values of 1 and 0, respectively, in the high field strength limit. That is, the saturated satellite initial state loses 100% of its enhancement in the high field strength limit, and, even worse, the inverted satellite initial state loses 150%. Similar to the equilibrium initial state, both saturated and inverted initial state signals fall half the distance to their minimum value at $\omega_1 \approx \omega_q/4$. Perhaps, more disturbing is that the enhanced signals have already decreased ~5% by $\omega_1 \approx \omega_q/48$. Since the equilibrium signal strength has also increased ~5% at the higher field strength, the overall enhancement, as calculated with Eq. (1), has decreased by ~10% by $\omega_1 \approx \omega_q/48$ for both the saturated and inverted satellite initial states.

As discussed earlier, much of the signal loss at higher rf field strengths can be avoided if the conversion pulse length is optimized on the enhanced initial state. This approach is adopted for the simulated signals shown in Fig. 5B. The signal strengths from a saturated and inverted initial state begin at their maximum values of ~2 and ~3, respectively, but now only decrease to minimum values of 1.78 (22% loss) and 2.32 (34% loss), respectively, in the high field strength limit.

In Fig. 6 is a comparison of the ^{23}Na experimental signal strengths in $NaNO_3$ as a function of rf field strength for the equilibrium and the saturated and inverted satellite initial states. The conversion pulse durations were optimized on the equilibrium magnetization in Fig. 6A and on the enhanced magnetization in Fig. 6B. To calibrate the experimental signal strength of the central transition, the intensity of the equilibrium spectra at the low rf field limit (660 Hz) was set to 1 and all other spectra were scaled to this. As predicted the equilibrium signal strength increased from 1 at low rf fields to almost 2 at high rf fields. The signal strength for FSG-RAPT and WURST populations in Fig. 6A, decreased from 1.78 and 2.32, respectively, at the lowest rf field strength to 1.06 and 0.55, respectively, at the highest rf field strength. When the conversion pulse length is optimized on the enhanced populations, as shown in Fig. 6B, the loss of signal for the enhanced populations is not as great in the high field strength limit, with signal for FSG-RAPT and WURST populations only decreasing to 1.54 and 1.88, respectively.

Also shown in Fig. 6 are the predicted signal strengths from full density matrix simulations using ideally enhanced initial states. Although the range of experimental signal strengths are not as great as the ideally enhanced states, due in part to the strong dipolar coupling between sodium nuclei, the trends with increasing rf field strength are the same, and there is very good agreement with the predicted crossing point, $\omega_1 \approx \omega_q/4$, where the enhancements have fallen half the distance to their minimum value.

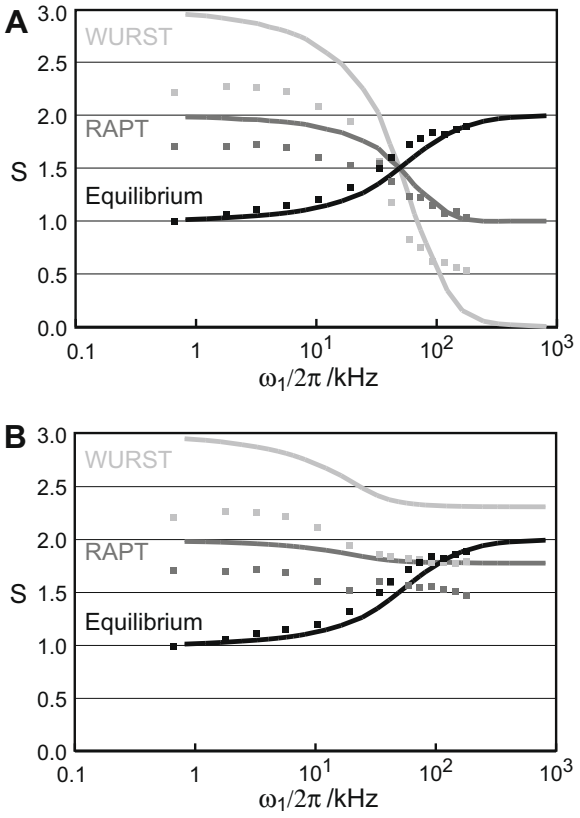

Fig. 6. (A) Experimental (square symbols) rf field dependence on the signal strength of the central transition of ^{23}Na in $NaNO_3$ with $\omega_q/2\pi \approx 170$ kHz. Experimentally, the maximum enhancements obtained with WURST (inversion) and RAPT (saturation) are 2.2 and 1.8, respectively. Simulated curves (solid lines) are for ideal equilibrium (black), saturated (grey) and inverted (light grey) initial density operators. Pulse lengths were optimized on the equilibrium populations. (B) Same as (A) except the pulse lengths were optimized on the enhanced populations.

4. Summary

We have shown that the central transition signal enhancement from selective satellite saturation or inversion sequences can be lost without proper optimization of the pulse that converts the enhanced central transition polarization into detectable coherence. While it is generally understood that central transition conversion pulse length requires careful optimization due to the complex dependence of its nutation frequency on the ω_q as well as ω_1, it is not generally realized that quadrupole nuclei evolving under identical Hamiltonians, i.e., having identical ω_1 and ω_q values but different initial polarizations will have different nutation frequencies (spectra) depending on the spin order ranks contained within the initial polarization. Thus, an important conclusion of this work is that a central transition pulse length optimized on equilibrium magnetization may not provide the maximum central transition sensitivity when applied to an enhanced (non-equilibrium) magnetization.

Even with optimization of the pulse length, the maximum possible enhancement decreases as the field strength of the conversion pulse increases from the low field strength ($\omega_1 \ll \omega_q$), to high field strength ($\omega_1 \gg \omega_q$) limit. A 10% loss in the overall enhancement is seen at values of $\omega_1 \approx \omega_q/48$ and losses continue to increase with increasing ω_1. Of course, in the very low rf field strength limit there will also be signal loss and distortion if the pulse does not exceed the necessary bandwidth to excite a central transition with a given offset and linewidth, that is, $\omega_1 > \Delta\Omega + \omega_q^2/\omega_0$. Thus, the conversion pulse field strength needs to be optimized to find a balance between these two limits. Such constraints suggest the use of shaped conversion pulses for enhanced populations, and further work along those lines is in progress in our laboratory.

Acknowledgments

This material is based upon work supported in part by the National Science Foundation under Grant No. CHE 0616881. This work was supported in part by an allocation of computing time from the Ohio Supercomputer Center.

Appendix A

In the high temperature approximation, the NMR equilibrium density operator is given by

$$\hat{\rho}_{eq} \approx \frac{\widehat{E} + \hbar\gamma B_0 \widehat{I}_z/k_B T}{\mathrm{Tr}\left(\widehat{E}\right)} = \frac{\widehat{E}}{k_B T(2I+1)} + \frac{\hbar\gamma B_0 \widehat{I}_z}{k_B T(2I+1)}. \tag{11}$$

Since $\widehat{E}$ is invariant under evolution, we can ignore it, writing the relevant part of the equilibrium density operator for our discussion as

$$\hat{\rho}_{eq} \approx b\widehat{I}_z, \tag{12}$$

where $b = \hbar\omega_0/k_B T(2I+1)$.

During an rf pulse the density operator in the rotating frame for a quadrupole nucleus evolves, to a first-order approximation, under the Hamiltonian

$$\widehat{H}/\hbar = \omega_q A_{20} \widehat{T}_{20} - \omega_1 \widehat{I}_x. \tag{13}$$

After an rf pulse of duration τ_p the density operator is given by

$$\rho(\tau_p) = \widehat{U}(\tau_p)\rho(0)\widehat{U}^\dagger(\tau_p), \tag{14}$$

where

$$\widehat{U}(\tau_p) = e^{-i\widehat{H}\tau_p/\hbar}, \tag{15}$$

and the (phase shifted) observable signal given by

$$S(\tau_p) = -i\mathrm{Tr}\left[\rho(\tau_p)\widehat{I}_+\right]. \tag{16}$$

When the size of the first-order quadrupole splitting of half-integer quadrupole nuclei exceeds the receiver bandwidth, then only the central $\frac{1}{2} \rightarrow -\frac{1}{2}$ transition is detected. This can be described in terms of fictitious spin-half operators [11,12], writing $\widehat{I}_+$ as

$$\widehat{I}_+ = \sum_{(r-s)^1} \sqrt{I(I+1) - m_r m_s}\, \widehat{I}_+^{r-s}, \tag{17}$$

where the summation is restricted to all ordered pairs of single quantum transitions. The detected signal then becomes

$$S(\tau_p) \approx -2i\mathrm{Tr}\left[\rho(\tau_p)\widehat{I}_+^{CT}\right], \tag{18}$$

where $\widehat{I}_+^{CT}$ is the fictitious spin half operator associated with the central $m = \frac{1}{2} \rightarrow -\frac{1}{2}$ transition. Substituting Eq. (14), the nutation signal becomes

$$S(\tau_p) \approx -2i\mathrm{Tr}\left[\rho(0)\widehat{U}^\dagger(\tau_p)\widehat{I}_+^{CT}\widehat{U}(\tau_p)\right]. \tag{19}$$

A.1. Low rf power regime

Writing the Hamiltonian in Eq. (13) in terms of fictitious spin half operators [11,12], yields

$$\widehat{H}/\hbar = \omega_q A_{20}\widehat{T}_{2,0} - \omega_1 \sum_{(r-s)^1} \sqrt{I(I+1) - m_r m_s}\,\widehat{I}_x^{r-s}. \tag{20}$$

When the size of the first-order quadrupole splitting exceeds the strength of the rf pulse field strength, i.e., $\omega_1 \ll \omega_q$, this Hamiltonian can be approximated to first order [13,11] in ω_1 as

$$\widehat{H}/\hbar \approx \omega_q A_{20}\widehat{T}_{2,0} - \left(I+\frac{1}{2}\right)\omega_1 \widehat{I}_x^{CT}, \tag{21}$$

and the propagator $\widehat{U}(\tau_p)$ becomes,

$$\widehat{U}(\tau_p) = e^{-i\omega_q A_{20}\widehat{T}_{2,0}\tau_p} e^{i(I+\frac{1}{2})\omega_1 \widehat{I}_x^{CT}\tau_p}. \tag{22}$$

Since $\left[\widehat{T}_{2,0}, \widehat{I}_+^{CT}\right] = 0$, we find the well-known result that the central transition in the low rf field strength limit nutates at a frequency of $(I+\frac{1}{2})\omega_1$ for spin I. Substituting Eq. (22) into Eq. (19) one obtains Eq. (5) for the case of $I = 3/2$.

A.2. High rf power regime

When the strength of the rf pulse field strength exceeds the size of the first-order quadrupole splitting, $\omega_1 \gg \omega_q$, the Hamiltonian can be approximated to lowest order as

$$\widehat{H}/\hbar \approx -\omega_1 \widehat{I}_x, \tag{23}$$

and the propagator $\widehat{U}(\tau_p)$ becomes,

$$\widehat{U}(\tau_p) = e^{i\omega_1\tau_p \widehat{I}_x} = \mathscr{D}\left(\frac{\pi}{2}, \omega_1\tau_p, -\frac{\pi}{2}\right), \tag{24}$$

where $\mathscr{D}$ is the Wigner rotation operator. In this limit we find it convenient to expand the observable operator, as well as the initial density operators before and after a CT population enhancement in terms of unit irreducible tensor operators, $\widehat{\mathscr{T}}_{l,m}$, which satisfy the trace relation

$$\mathrm{Tr}\left[\widehat{\mathscr{T}}_{l,m}\widehat{\mathscr{T}}^{\dagger}_{l',m'}\right] = \delta_{l,l'}\delta_{m,m'}. \tag{25}$$

It is important not to confuse these operators with the non-unit irreducible tensor operators, $\widehat{T}_{l,m}$, which are more commonly used in theoretical descriptions of NMR Hamiltonians. The relationship between the unit, $\widehat{\mathscr{T}}_{l,m}$, and non-unit, $\widehat{T}_{l,m}$, tensor operators is given by [14]

$$\widehat{\mathscr{T}}_{l,m} = \frac{1}{l!}\left[\frac{(2l+1)(2I-l)!2^l(2l)!}{(2I+l+1)!}\right]^{1/2}\widehat{T}_{l,m}. \tag{26}$$

Using the expression [15,16]

$$|j\rangle\langle i| = \sum_{L=0}^{2I}\sqrt{\frac{2L+1}{2I+1}}\langle Ij|IL\,ij-i\rangle\widehat{\mathscr{T}}_{L,j-i}, \tag{27}$$

we expand the central transition observable, $\widehat{I}_+^{CT}$, as

$$\widehat{I}_+^{CT} = \left|\frac{1}{2}\right\rangle\left\langle -\frac{1}{2}\right| = \sum_{L=1}^{2I}\sqrt{\frac{2L+1}{2I+1}}\left\langle I\frac{1}{2}\middle| IL\,-\frac{1}{2}\,1\right\rangle\widehat{\mathscr{T}}_{L,1}. \tag{28}$$

After a population transfer sequence the density operator can be expanded as

$$\widehat{\rho}(0) = \frac{\widehat{E}}{k_B T(2I+1)} + \sum_{L=1}^{2I}\rho_L(0)\widehat{\mathscr{T}}_{L,0}, \tag{29}$$

where

$$\rho_L(0) = \mathrm{Tr}\left[\hat{\rho}(0)\,\widehat{\mathscr{T}}^{\dagger}_{L,0}\right]. \tag{30}$$

Table 1
Reduced Wigner rotation matrix elements, $d^L_{1,0}(\beta)$ up to $L = 9$.

L	$d^L_{1,0}(\beta)\cdot 2^L\cdot\sqrt{2}$
1	$-2\sin\beta$
2	$-2\sqrt{3}\sin 2\beta$
3	$-\frac{\sqrt{6}}{2}(\sin\beta - 5\sin 3\beta)$
4	$-\frac{\sqrt{5}}{2}(2\sin 2\beta + 7\sin 4\beta)$
5	$-\frac{\sqrt{15}}{4}(2\sin\beta + 27\sin 3\beta + \sin 5\beta)$
6	$-\frac{\sqrt{21}}{4}(5\sin 2\beta + 12\sin 4\beta + 33\sin 6\beta)$
7	$-\frac{33\sqrt{7}}{16}(\frac{25}{33}\sin\beta + \frac{81}{33}\sin 3\beta + 5\sin 5\beta + 13\sin 7\beta)$
8	$-\frac{429}{16}(\frac{70}{143}\sin 2\beta + \frac{14}{13}\sin 4\beta + 2\sin 6\beta + 5\sin 8\beta)$
9	$-\frac{429\sqrt{5}}{64}(\frac{98}{143}\sin\beta + \frac{28}{13}\sin 3\beta + 4\sin 5\beta + 7\sin 7\beta + 17\sin 9\beta)$

For the equilibrium density operator this expansion will contain only an $L = 1$ contribution. After selective saturation or selective inversion of satellite transition pairs, i.e., $m \leftrightarrow m-1$ and $-m \leftrightarrow -m+1$, the density operator, $\hat{\rho}(0)$, can contain contributions from all odd values of L up to $L = 2I$.

Substituting Eqs. (24), (28), and (29) into Eq. (19) we obtain

$$S(\tau_p) \approx 2\sum_{L=0}^{2I}\sqrt{\frac{2L+1}{2I+1}}\left\langle I\frac{1}{2}\middle| IL\,-\frac{1}{2}\,1\right\rangle\rho_L(0)\,d^{(L)}_{1,0}(\omega_1\tau_p), \tag{31}$$

where $d^{(L)}_{1,0}(\beta)$ is the reduced Wigner rotation matrix, which are given in Table 1 for $L = 1$ to $L = 9$ to describe the nutation behavior spin $I = 1$ to $I = 9/2$.

References

[1] Z. Yao, H.-T. Kwak, D. Sakellariou, L. Emsley, P.J. Grandinetti, Sensitivity enhancement of the central transition NMR signal of quadrupolar nuclei under magic-angle spinning, Chem. Phys. Lett. 327 (2000) 85–90.
[2] S. Prasad, H.T. Kwak, T. Clark, P.J. Grandinetti, A simple technique for determining nuclear quadrupole coupling constants using RAPT solid-state NMR spectroscopy, J. Am. Chem. Soc. 124 (18) (2002) 4964–4965.
[3] H.-T. Kwak, S. Prasad, T.M. Clark, P.J. Grandinetti, Enhancing sensitivity of quadrupolar nuclei in solid-state NMR with multiple rotor assisted population transfers, Solid-State NMR 24 (2003) 71–77.
[4] D. Iuga, H. Schafer, R. Verhagen, A. Kentgens, Population and coherence transfer induced by double frequency sweeps in half-integer quadrupolar spin systems, J. Magn. Reson. 147 (2000) 192–209.
[5] S. Vega, Y. Naor, Triple quantum NMR on spin systems with $I = 3/2$ in solids, J. Chem. Phys. 75 (1981) 75.
[6] R. Siegel, T.T. Nakashima, R.E. Wasylishen, Signal enhancement of NMR spectra of half-integer quadrupolar nuclei in solids using hyperbolic secant pulses, Chem. Phys. Lett. 388 (2004) 441–445.
[7] K.K. Dey, S. Prasad, J.T. Ash, M. Deschamps, P.J. Grandinetti, Spectral editing in solid-state MAS NMR of quadrupolar nuclei using selective satellite inversion, J. Magn. Reson. 185 (2007) 326–330.
[8] M.A. Eastman, P.J. Grandinetti, Y.K. Lee, A. Pines, Double-tuned hopping-coil probe for dynamic-angle spinning NMR, J. Magn. Reson. 98 (1992) 333–341.
[9] N.M. Trease, P.J. Grandinetti, Solid-state nuclear magnetic resonance in the rotating tilted frame, J. Chem. Phys. 128 (5) (2008) 052318.
[10] A. Samoson, E. Lippmaa, 2D NMR nutation spectroscopy in solids, J. Magn. Reson. 79 (2) (1988) 255–268.
[11] S. Vega, Fictitious spin-1/2 operator formalism for multiple quantum NMR, J. Chem. Phys. 68 (1978) 5518–5527.
[12] A. Wokaun, R.R. Ernst, Selective excitation and detection in multilevel spin systems: application of single transition operators, J. Chem. Phys. 67 (1977) 1752–1758.
[13] H.-T. Kwak, S. Prasad, Z. Yao, P.J. Grandinetti, J.R. Sachleben, L. Emlsey, Enhanced sensitivity in RIACT/MQ-MAS NMR experiments using rotor assisted population transfer, J. Magn. Reson. 150 (2001) 71–80.
[14] G.J. Bowden, W.D. Hutchison, Tensor operator formalism for multiple-quantum NMR. 1. Spin-1 nuclei, J. Magn. Reson. 67 (1986) 403–414.
[15] M.E. Rose, Elementary Theory of Angular Momentum, Wiley, New York, 1955.
[16] D.A. Varshalovich, A.N. Moskalev, V.K. Khersonskii, Quantum Theory of Angular Momentum, World Scientific, Teaneck, NJ, 1988.